AxTract: Toward Microstructure Informed Tractography

Gabriel Girard*[1,2,3], Alessandro Daducci[4,5,3], Laurent Petit[6], Jean-Philippe Thiran[3,5], Kevin Whittingstall[7,8], Rachid Deriche[2], Demian Wassermann†[2] and Maxime Descoteaux†[1,8,3]

[1] *Sherbrooke Connectivity Imaging Lab, Computer Science Department, Faculty of Science, Université de Sherbrooke, Canada*

[2] *Project Team Athena, INRIA Sophia Antipolis Méditerranée, France*

[3] *Signal Processing Lab (LTS5), École Polytechnique Fédérale de Lausanne, Switzerland*

[4] *Computer Science Department, University of Verona, Italy*

[5] *Radiology Department, Centre Hospitalier Universitaire Vaudois and University of Lausanne, Switzerland*

[6] *Groupe d'Imagie Neurofonctionnelle, Institut des Maladies Neurodégénératives - UMR 5293, CNRS, CEA University of Bordeaux, France*

[7] *Department of Diagnostic Radiology, Faculty of Medicine and Health Science, Université de Sherbrooke, Canada*

[8] *Sherbrooke Molecular Imaging Center, Department of Nuclear Medicine and Radiobiology, Faculty of Medicine and Health Science, Université de Sherbrooke, Canada*

Abstract

Diffusion-weighted (DW) magnetic resonance imaging (MRI) tractography has become the tool of choice to probe the human brain's white matter *in vivo*. However, tractography algorithms produce a large number of erroneous streamlines (false positives), largely due to complex ambiguous tissue configurations. Moreover, the relationship between the resulting streamlines and the underlying white matter microstructure characteristics remains poorly understood. In this work, we introduce a new approach to simultaneously reconstruct white matter fascicles and characterize the apparent distribution of axon diameters within fascicles. To achieve this, our method, *AxTract*, takes full advantage of the recent development DW-MRI microstructure acquisition, modelling and reconstruction techniques. This enables *AxTract* to separate parallel fascicles with different microstructure characteristics, hence reducing ambiguities in areas of complex tissue configuration. We report a decrease in the incidence of erroneous streamlines compared to the conventional deterministic tractography algorithms on simulated data. We also report an average increase in streamline density over 15 known fascicles of the 34 healthy subjects. Our results suggest that microstructure information improves tractography in crossing areas of the white matter. Moreover, *AxTract* provides additional microstructure information along the fascicle that can be studied alongside other streamline-based indices. Overall, *AxTract* provides the means to distinguish and follow white matter fascicles using their microstructure characteristics, bringing new insights into the white matter organization. This is a step forward in microstructure informed tractography, paving the way to a new generation of algorithms able to deal with intricate configurations of white matter fibres and providing quantitative brain connectivity analysis.

Key words: White Matter Tractography, Diffusion MRI, Microstructure, Axon Diameter Index, ActiveAx, Multi-Shell Acquisition

*Corresponding author: gabriel.p.girard@usherbrooke.ca

†These authors contributed equally

Introduction

Diffusion-weighted (DW) magnetic resonance imaging (MRI) tractography has become the tool of choice to probe the human brain's white matter *in vivo*. Recent results have shown that, albeit tractography can extract large white matter fascicles from DW-MRI, there is a high incidence of erroneous streamlines (false positives) resulting from current tractography algorithms [Côté et al., 2013; Jbabdi et al., 2015; Jones, 2010; Maier-Hein et al., 2016; Thomas et al., 2014]. This is largely due to complex ambiguous local fibre configurations (e.g. crossing, kissing or fanning) [Maier-Hein et al., 2016; Savadjiev et al., 2014]. Furthermore, the relationship between the resulting streamlines and the underlying white matter microstructure characteristics, such as axon diameter, remains poorly understood [Jones, 2010].

Recently, microstructure imaging has recently become one of the main topics in DW-MRI technology development. The lack of specificity of diffusion tensor imaging measures such as fractional anisotropy [Jones, 2010] combined with the sensitivity of these measures to changes in several white matter pathologies [e.g. Jolles et al., 2016; Matsui et al., 2015; Song et al., 2005] has generated the need for measures that are in closer relationship with white matter tissue changes [Alexander et al., 2010]. Currently, the microstructure imaging field is parted. On one hand, there is an emergence of approaches claiming that interpretability of the DW-MRI signal will be achieved faster by analysing the extra-cellular space and quantifying phenomena such as changes in axonal packing [e.g. Burcaw et al., 2015; Novikov et al., 2014; Sepehrband et al., 2015]. On the other hand, there is a growing effort to take advantage of novel high-end MRI systems to measure the restricted intra-cellular diffusivity and quantify microstructure [Alexander et al., 2010; Assaf and Basser, 2005; Assaf et al., 2008; Barazany et al., 2011; Daducci et al., 2015; Fick et al., 2016; Huang et al., 2015; Kaden et al., 2015; Özarslan et al., 2013; Panagiotaki et al., 2012; Raffelt et al., 2012; Reisert et al., 2014; Scherrer et al., 2015; Zhang et al., 2011a,b, 2012]. Complementary to these two trends, there is a need to take advantage of these technologies at the tractography algorithm level. Post-processing approaches have been proposed to combine microstructure information and tractography [Amitay et al., 2016; Barakovic et al., 2016; Daducci et al., 2014, 2016, 2013; Pestilli et al., 2014; Sherbondy et al., 2010; Smith et al., 2013]. To solve complex white matter areas (e.g. crossing, kissing or fanning fibre configurations), these approaches use a precomputed set of streamlines to estimate microstructure information and to reject (or penalized) erroneous streamlines from a full brain tractography reconstruction. This is sensitive to the choice of the tractography algorithm used, since these approaches can only filter out unlikely streamlines and they require the tractography algorithm to provide a dense sample of all streamline configurations inside complex regions.

In this work, we introduce a new algorithm, *AxTract* (*Axon/ActiveAx Tractography*), to reconstruct white matter fascicles while simultaneously characterizing the apparent distribution of axon diameters within fascicles. To achieve this, our method takes full advantage of current DW-MRI microstructure models [e.g. Alexander et al., 2010; Daducci et al., 2015; Huang et al., 2015; Panagiotaki et al., 2012; Scherrer et al., 2015; Zhang et al., 2011a,b]. The distinctive aspect of our tractography algorithm from previous methods is the active use of a microstructure tissue model to estimate and exploit microstructure information about fascicles during the tracking process. This allows us to reduce ambiguities in areas of complex tissue configuration and separate parallel fascicles with different microstructure characteristics, hence improving the overall tractography process.

Materials and methods

AxTract: microstructure informed tractography

The main purpose of our novel tractography algorithm, *AxTract*, is to simultaneously estimate the trajectories of the white matter fibres and their microstructure features (e.g. diameter). The main hypothesis driving *AxTract* is that the mean diameter of the axons composing a fascicle varies slowly along its pathway [Debanne et al., 2011; Liewald et al., 2014; Ritchie, 1982]. To formulate our algorithm, we start from the classical equation driving discrete deterministic streamline tractography [Basser et al., 2000]:

$$\boldsymbol{r}_{i+1} = \boldsymbol{r}_i + \Delta s \; \boldsymbol{t}_i, \tag{1}$$

where the sequence of 3D points $\rho = [\boldsymbol{r}_0, \ldots, \boldsymbol{r}_n]$ is the streamline tracking the white matter fascicle starting at the initial position $\boldsymbol{r}_0$ and following the direction $\boldsymbol{t}_i$, the tangent vector to the fascicle at the position $\boldsymbol{r}_i$, until a stopping criteria is reached (e.g. exiting the tracking mask). The streamline ρ is estimated using a fixed step size Δs. Using the diffusion tensor [Basser et al., 2000], $\boldsymbol{t}_i$ is taken to be the eigenvector corresponding to the maximal eigenvalue at the position $\boldsymbol{r}_i$. Generally, tractography algorithms based on the diffusion tensor rely on the hypothesis that white matter fibres are locally tangent to the direction of maximal diffusivity. Specifically, the diffusion tensor model cannot express complex geometries such as white matter fascicles crossings and kissings [Behrens et al., 2007]. Hence, several algorithms have been proposed to extend this algorithm and be able to trace through these geometries [e.g. Dell'Acqua et al., 2007; Descoteaux et al., 2007, 2009; Malcolm et al., 2010; Tournier et al., 2007, 2012; Tristán-Vega et al., 2009; Tuch, 2004]. In these approaches, $\boldsymbol{t}_i$ is one direction d from the set of local maxima (or peaks) of a spherical function (SF), e.g. the diffusion orientation distribution function (ODF) or the fibre ODF, describing orientations of the tissues :

$$\boldsymbol{t}_i \in \arg\max_{\boldsymbol{d}} \; \mathrm{SF}_{\boldsymbol{r}_\mathrm{i}}(\mathrm{d}), \tag{2}$$

where $\boldsymbol{r}_i$ is the tracking position. Deterministic tractography algorithms rely on the same hypothesis that the peaks are sufficient to trace fascicles and add, in one way or another, a new hypothesis of preservation of the previous tracking direction $\boldsymbol{t}_{i-1}$. In most cases, if more than one tracking direction is available, $\boldsymbol{t}_i$ is chosen to minimize the angular deviation from the previous direction $\boldsymbol{t}_{i-1}$. The tracking direction $\boldsymbol{t}_i$ is selected from the M directions $\boldsymbol{d}_m$ corresponding to the peaks of SF following:

$$\boldsymbol{t}_i = \arg\min_{\boldsymbol{d}_m} \; \arccos\left(\boldsymbol{t}_{i-1} \cdot \boldsymbol{d}_m\right), \quad \boldsymbol{d}_m \in [\boldsymbol{d}_1, \; \ldots, \; \boldsymbol{d}_M], \quad \text{s.t.} \;\; \arccos\left(\boldsymbol{t}_{i-1} \cdot \boldsymbol{d}_m\right) < \theta. \tag{3}$$

Moreover, $\boldsymbol{d}_m$ is constrained to form an angle smaller than θ with the previous direction $\boldsymbol{t}_{i-1}$ to enforce smoothness in the streamline ρ.

With *AxTract*, we aim at preserving coherence in the direction and in the axon diameter, adding a biologically-driven hypothesis. This enables the deterministic tractography to traverse complex structures by selecting propagation directions using additional information [Debanne et al., 2011; Liewald et al., 2014; Ritchie, 1982]. Using *AxTract*, the definition of $\boldsymbol{t}_i$ in Equation 3 becomes:

$$\boldsymbol{t}_i = \arg\min_{\boldsymbol{d}_m} \; \|\alpha_\rho - \alpha_{\boldsymbol{d}_m}\|^2, \quad \boldsymbol{d}_m \in [\boldsymbol{d}_1, \; \ldots, \; \boldsymbol{d}_M], \quad \text{s.t.} \;\; \arccos\left(\boldsymbol{t}_{i-1} \cdot \boldsymbol{d}_m\right) < \theta, \tag{4}$$

where $\alpha_{\boldsymbol{d}_m}$ is the estimated axon diameter index in direction $\boldsymbol{d}_m$ and α_ρ is the estimated local axon

diameter index of the streamline ρ (the axon diameter index α is defined in the section below). Equation 4 allows tractography to follow the direction with the axon diameter index the closest to the one of the current streamline. Additionally, Equation 4 constraints the selected direction to form an angle smaller than θ with the previous direction $\boldsymbol{t}_{i-1}$ to enforce a low curvature in the streamline ρ.

Implementation details

In this work, we formulated our streamline propagation algorithm, *AxTract*, to follow both smooth trajectories and consistent axonal fascicle diameter characteristics. Several multi-compartment white matter models have been proposed to obtain microstructure characteristics from DW-MRI [e.g Alexander et al., 2010; Assaf and Basser, 2005; Assaf et al., 2008; Panagiotaki et al., 2012; Scherrer et al., 2015; Zhang et al., 2011a,b]. *AxTract* is not dependent on a specific white matter model, but requires a model capable to distinguish axon diameter characteristics in voxels with multiple fibre populations, i.e. with multiple peaks. In Dyrby et al. [2012], authors showed that the *ActiveAx* model [Alexander et al., 2010] can reproducibly distinguish average axon diameter characteristics using feasible acquisition protocols. Moreover, Zhang et al. [2011a] showed that the *ActiveAx* model can be extended to multiple fibre populations per voxel, providing an estimate of the axon diameter index per fiber population. In Auría et al. [2015], authors showed that *ActiveAx* model with multiple fibre populations per voxel can be efficiently computed using the peaks of the fibre ODF as input directions for the fibre populations. They showed that the axon diameter characteristics of each fibre population can be efficiently recovered with up to three fibre populations per voxel (i.e. 1, 2 or 3 fibre ODF peaks). We thus based our local microstructure estimation problem using the *ActiveAx* model [Alexander et al., 2010] generalized to multiple fibre populations per voxel [Auría et al., 2015; Zhang et al., 2011a] implemented in the efficient *AMICO* framework (Accelerated Microstructure Imaging via Convex Optimization) [Daducci et al., 2015]. Details of the axon diameter index estimation using *AMICO* are presented in Appendix A.

At each point along the streamline, we first interpolate linearly the spherical harmonic coefficients of the fibre ODF [Descoteaux et al., 2009; Tournier et al., 2007] to extract the fibre ODF peaks at the current position. Then, we interpolate linearly the DW-MRI signal and use *AMICO* [Auría et al., 2015] to estimate the axon diameter index $\alpha_{\boldsymbol{d}_m}$ for each direction $\boldsymbol{d}_m$ corresponding to the peaks. Following Equation 4, the streamline propagates in the direction with the axon diameter index $\alpha_{\boldsymbol{d}_m}$ the closest to the current approximation of the streamline axon diameter index α_ρ and with a maximum deviation angle of $\theta = 45°$ [Girard et al., 2014; Tournier et al., 2012]. The approximation of the streamline axon diameter index α_ρ is constantly updated from the median α over a fixed distance of $5cm$ of the current tracking position to account for variability along the fascicle (e.g. fanning, kissing, branching). If the current streamline length is less then $5cm$, all previous tracking positions are use to estimate α_ρ. We supposed that the median over a short distance from the tracking position provides information on the fascicle microstructure, while allowing for smooth changes along the fascicle.

Streamlines propagation stops when a position outside the white matter volume is reached. To allow streamlines to propagate through voxels with missing directions (e.g. due to noise in the DW-MRI images) and reach the grey matter, streamlines follow the previous tracking direction $\boldsymbol{t}_{i-1}$ when there is no direction available (i.e. no peak in the cone defined by the angle θ) [Girard et al., 2014; Weinstein et al., 1999]. The propagation stops after a distance of $2mm$ without available direction [Girard et al., 2014]. The initial tracking direction $\boldsymbol{t}_0$ is randomly chosen from the directions belonging the fibre ODF peaks at the initial position $\boldsymbol{r}_0$. A streamline is formed from the two independent trajectories obtained following both the initial direction and its opposite. For both trajectories, α_ρ is initiated to

the axon diameter index of the initial direction. The tracking step size Δs is fixed to $0.5mm$ [Girard et al., 2014; Tournier et al., 2012].

Dataset and experiments

AxTract streamlines are compared to the same deterministic tractography algorithm without using the axon diameter index information, referred as conventional deterministic tractography (CDT). The only difference between *AxTract* and CDT is thus the selection of the propagation direction at tracking positions with more than one valid direction: CDT always selects the propagation direction $\boldsymbol{d}_m$ that minimize the curvature of the streamline (Equation 3), *AxTract* selects the propagation direction $\boldsymbol{d}_m$ with $\alpha_{\boldsymbol{d}_m}$ the closest to the axon diameter index α_ρ of the streamline (Equation 4).

Simulated dataset

We used *Phantomas* [Caruyer et al., 2014] to generate a kissing configuration between two fascicles, from which, fascicle directions were obtained at each voxel. For each fascicle direction, the DW-MRI signal was independently simulated for a gamma distribution, $\Gamma(shape, scale)$, of parallel cylinders diameter, with a fixed distinct mean diameter per fascicle of $\alpha = 2.44\mu m$ ($\Gamma_{shape} = 5.3316$, $\Gamma_{scale} = 1.0242\times10^{-7}$, *Camino* substrate *AbR1a*), and $\alpha = 6.88\mu m$ ($\Gamma_{shape} = 5.3316$, $\Gamma_{scale} = 2.0484\times10^{-7}$, *Camino* substrate *AbD1a*) [Alexander et al., 2010; Assaf et al., 2008; Auría et al., 2015; Hall and Alexander, 2009; Liewald et al., 2014]. The simulated DW-MRI images were generated with the *in vivo* MGH-USC HCP imaging protocol (552 volumes, b-values up to $10,000s/mm^2$, $\delta = 12.9ms$, $\Delta = 21.8ms$), using the *Camino* [Hall and Alexander, 2009] Monte-Carlo diffusion simulator. The simulated signal was contaminated with Rician noise [Gudbjartsson and Patz, 1995] at signal to noise ratio (SNR) 10, 20 and 30.

Tractography was initiated both from fascicles interfaces (100 streamlines per voxel; 18,800 streamlines overall) or from all voxels of the white matter volume (20 streamlines per voxel; 22,400 streamlines overall). To evaluate reconstructed streamlines, we used the *Tractometer* [Côté et al., 2013] connectivity analysis. We report the following *Tractometer* metrics:

- *Valid Connections (VC)*: streamlines connecting expected regions of interest (ROIs) and not exiting the expected fascicle volume [Côté et al., 2013],
- *Invalid Connections (IC)*: streamlines connecting unexpected ROIs or streamlines connecting expected ROIs but exiting the expected fascicle volume. These streamlines are spatially coherent, have managed to connect ROIs, but do not agree with the ground truth [Côté et al., 2013],
- *No Connections (NC)*: streamlines not connecting two ROIs. These streamlines either stop prematurely due to angular constraints or exit the boundaries of the tracking volume [Côté et al., 2013],

In vivo dataset

We used the MGH-USC Human Connectome Project (HCP) adult diffusion dataset (34 subjects) [Fan et al., 2016; Keil et al., 2013; Setsompop et al., 2013]. The DW-MRI acquisition scheme consists of 552 volumes with b-values up to $10,000s/mm^2$, including 40 non-diffusion (b-value = 0) images. The DW-MRI images were acquired at $1.5mm$ isotropic voxel size using a Spin-echo EPI sequence ($TR/TE = 8800/57ms$, $\delta = 12.9ms$, $\Delta = 21.8ms$). We used the provided pre-processed DW-MRI images corrected for motion and EDDY currents [Andersson et al., 2012; Fan et al., 2016; Greve and Fischl, 2009]. Diffusion Tensor estimation and corresponding fractional anisotropy map generation

were done using *Dipy* [Garyfallidis et al., 2014]. From this, a single averaged fibre response function was estimated in fractional anisotropy values above a threshold of 0.7, within the white matter volume, from all subjects. The fibre response was used as input for spherical deconvolution [Raffelt et al., 2012; Tournier et al., 2007] to compute the fibre ODFs using DW-MRI images of a single b-value shell of $3000 s/mm^2$ (maximum spherical harmonic order 8). A T1-weighted $1mm$ isotropic resolution 3D MPRAGE (TR/TE/TI 2530/1.15/1100 ms) image was also acquired [Fan et al., 2016]. The T1-weighted image was first registered to the DW-MRI images using ANTs [Avants et al., 2009]. The brain parcellation was then obtained using *FreeSurfer* [Salat et al., 2009] and white matter volume was obtained using *FSL/FAST* [Zhang et al., 2001]. T1-weighted images were also registered to the *ICBM 2009a Nonlinear Symmetric Atlas* [Fonov et al., 2011] for voxel-based group analysis. Five streamlines were initiated per voxel of the white matter volume. Fascicles were obtained using the *TractQuerier* [Wassermann et al., 2016] (see the supplementary material for the white matter fascicle definitions and queries). The mean axon diameter index α, the mean apparent fibre density (AFD, mean fibre ODF value along streamlines segments) [Dell'Acqua et al., 2010, 2013; Raffelt et al., 2012] and the mean fractional anisotropy are reported over all segments of all streamlines of each fascicles of the 34 subjects. We also report the percentage change in the number of streamlines [Catani et al., 2007; Lebel and Beaulieu, 2009; Thiebaut de Schotten et al., 2011; Vernooij et al., 2006] using *AxTract* compared to conventional deterministic tractography (CDT): $\frac{AxTract-CDT}{CDT} \times 100$. We used two-tailed t-tests with the Bonferroni correction ($p < 0.05$) to test for an increase or a decrease in the percentage change in the number of streamlines using *AxTract* with a null hypothesis of 0.

Results

Simulated data experiment

AxTract and conventional deterministic tractography reconstructions on the simulated kissing dataset (SNR=20) is shown in Figure 1. Figure 1 (a, b, c) shows the ground truth segment-wise directions used to generate the data, the estimated fibre ODFs and the fibre ODF peaks, respectively. Figure 1 (d) shows the fibre ODF peaks with their length scaled by the axon diameter index α. Figure 1 (e, f) show valid and invalid connections for both *AxTract* and conventional deterministic tractography. Table 1 reports the *Tractometer* connectivity evaluation on the simulated kissing configuration (SNR=10, 20, 30), initiating the tractography both from fascicles interfaces or from the white matter volume. *AxTract* produces 87.2% of valid connections compared to 52.5% using conventional deterministic tractography, with SNR=20 and initiating tractography at the interface (71.3% and 54.7%, respectively initiating from the white matter volume). The invalid connections decrease proportionally and the no connections stay similar for both *AxTract* and conventional deterministic tractography. Table 2 reports the mean and standard deviation of the axon diameter index α estimated along streamlines' segments (valid connections), for each fascicle. The mean axon diameter index α is similar for both interface and white matter volume tractography initializations and across SNRs. However, increasing the noise in the DW-MRI images increases the standard deviation of the estimated α for both fascicles. This perturbed the selection of the propagation direction by *AxTract*, which decreases the percentage of valid connections obtained with *AxTract*, from 90.5% at SNR=30 to 72.1% at SNR=10 initiating from fascicles extremities, respectively from 73.9% to 60.9% initiating from the white matter volume. However, those results are always higher for *AxTract* than for conventional deterministic tractography, which obtained 53.9% at SNR=30 and 55.9% at SNR=10 initiating from fascicles extremities, respectively 55.3% and 54.1% initiating from the white matter volume (see Table

1). The mean α of the right fascicles (the largest) is always underestimated and the mean α of the left fascicles (the smallest) is always overestimated.

In vivo data experiment

Figures 2 and 3 show the axon diameter index α obtained with *AxTract* along five white matter fascicles of one subject (mgh_1001): the arcuate fasciculus (AF), the corticospinal tract (CST), the inferior fronto-occipital fasciculus (IFOF), the superior longitudinal fasciculus (SLF) and the uncinate fasciculus (UF). In column 3, we report the histogram of axon diameter index α estimated at each segment of all streamlines of each fascicle (streamlines shown in column 2). In column 5, we report for each fascicle, the histogram of the whole-streamline median axon diameter index α (one value per streamline), for all streamlines (streamlines shown in column 4). Differences in the estimated axon diameter index α can be observed across fascicles in both histograms. Figure 4 shows the same information for the corpus callosum (CC). The corpus callosum is split in 5 sub-fascicles using the *FreeSurfer* parcellation and *TractQuerier* (anterior, mid-anterior, central, mid-posterior, posterior). A decrease in the percentage of segments with a high axon diameter index α can be observed in the posterior part of the corpus callosum. Figure 5 (a,b) shows the corpus callosum of the same subject with *AxTract* streamlines coloured using α estimated per segment and using the whole-streamline median α. The largest α (green) can be observed in the central part of the corpus callosum using segment-wise estimation. However, the trend disappears using the whole-streamline median estimation.

Figure 6 (a) shows the average occurrence map of *AxTract* selecting a different propagation direction than conventional deterministic tractography over the 34 subjects. *AxTract* changed the propagation direction more frequently in low angle crossing areas of the white matter. Areas with single fibre orientation or with multiple fibre orientations but not within the maximum deviation angle ($\theta = 45°$) from the propagating streamline, show no changes in propagation directions. Figure 6 (b,c,d) shows the segments of streamlines of three fascicles (AF, CST, UF) where such changes occurred for one subject (mgh_1001). During the tracking process of the 34 subjects, there were multiple propagation directions available in $2.5\% \pm 0.2$ of tracking steps ($\pm$ standard deviation). *AxTract* changed the propagation direction using the axon diameter index α in $19.0\% \pm 0.3$ of tracking steps with multiple directions available.

Finally, Figure 7 (a) shows the distributions of relative changes in streamlines count (%) between *AxTract* and conventional deterministic tractography, across fascicles of the 34 healthy subjects: the arcuate fasciculus (AF), the corticospinal tract (CST), the inferior fronto-occipital fasciculus (IFOF), the superior longitudinal fasciculus (SLF), the uncinate fasciculus (UF) and the corpus callosum (CC). We report a significant increase in streamlines count for the corticospinal tract (left: $T_{(33)} = 3.9,\ p = 7.5 \times 10^{-03}$, right: $T_{(33)} = 4.0,\ p = 5.4 \times 10^{-03}$) and for the corpus callosum (anterior: $T_{(33)} = 3.4,\ p = 2.9 \times 10^{-02}$, central: $T_{(33)} = 7.1,\ p = 6.8 \times 10^{-06}$, mid-posterior: $T_{(33)} = 5.9,\ p = 7.1 \times 10^{-07}$, posterior: $T_{(33)} = 3.1,\ p = 2.2 \times 10^{-05}$), and a significant decrease for the arcuate fasciculus (left: $T_{(33)} = -3.6,\ p = 2.4 \times 10^{-02}$). Across all selected fascicles, *AxTract* shows an average increase 6.3% in streamline count compared to conventional deterministic tractography. The distribution of mean α for the same fascicles is reported in Figure 7 (b). The mean apparent fibre density and the mean fractional anisotropy are shown as reference in Figures 7 (c, d). Projection and association fascicles are reported for each hemisphere. The profile of the distribution of the axon diameter index α, the apparent fibre density and the fractional anisotropy is different and values vary across fascicles, bringing complementary information on those fascicles.

Discussion

We introduced a novel tractography method, *AxTract*, which incorporates apparent axonal microstructure measurements to reconstruct white matter fascicles of the brain. Despite the current discussion on the feasibility of measuring axon diameters with DW-MRI [Alexander et al., 2010; Novikov et al., 2014], our results show that incorporating surrogate measures to axon diameter has a positive effect on tractography results. Specifically, we incorporated the axon diameter index α [Alexander et al., 2010] obtained from DW-MRI using the efficient implementation *AMICO* [Auría et al., 2015]. Using this technique, our algorithm can disentangle complex architecture based on microstructure characteristics. *AxTract* is able to distinguish white matter fascicles through their microstructure characteristics while being able to perform full brain tractography in reasonable time (approximately 72 hours for *AxTract* compared to 6 hours for the conventional deterministic tractography implementation, for 600,000 streamlines). Our results on simulated data show that *AxTract* is a promising approach to reduce the incidence of invalid connections produced by current tractography algorithms. Our results on *in vivo* data show that the axon diameter index α changed the direction of the tracking resulting in an overall increase of the amount of streamlines in the identified fascicles. In the absence of ground truth *in vivo* connectivity data, it is a challenge to show the increase of valid connections and decrease of invalid connections but, we show evidence that *AxTract* is a novel method taking a step in the right direction.

Reducing ambiguities in complex white matter architecture

AxTract distinguishes fascicles in complex architectures when these have different axon diameter. Specifically, in the crossing area on Figure 1, *AxTract* privileges following the direction which minimizes the deviation from axon diameter index α of the fascicle being reconstructed while the usual tractography approach is to minimize the angular deviation. In doing so, *AxTract* is able to better resolve the kissing configuration and decreases the percentage of invalid connections. Always following the direction with the lowest local angular deviation, as with conventional deterministic tractography, leads to errors in the kissing configuration reconstruction. This is quantitatively reported by the *Tractometer* [Côté et al., 2013] metrics in Table 1. *AxTract* always increases the valid connections and decreases the invalid connections compared to conventional deterministic tractography. The valid connections also increase with an increase in SNR for *AxTract*. The increase in valid connections is also higher for *AxTract* initiating the tractography from fascicle extremities, i.e. the white matter / grey matter interface. This is because the tracking starts in regions where α is specific of the fascicle, i.e. α_d estimated in the initial direction tend toward the ground truth α of the fascicle. This is not the case when the tracking starts in the central part of the dataset, where only one peak is obtained from the fibre ODF. Hence, *AMICO* estimates the axon diameter index in this single direction, despite the ground truth having two directions, see Figure 1 (a,c). Since the two ground truth directions are almost aligned, the axon diameter index tend towards the average α of both simulated fascicles. This makes *AxTract* unable to distinguish which direction to follow in subsequent tractography steps with multiple fibre ODF peaks. Nonetheless, *AxTract* performs similarly to the conventional deterministic tractography when initiated in regions where fascicles population cannot be distinguished. It is worth mentioning that two streamlines being reconstructed with *AxTract*, reaching the very same position and with the same previous tracking direction won't necessarily result in the same trajectory. Contrary to conventional deterministic tractography, *AxTract* uses the information from many previous tracking steps (up to $5cm$ with α_ρ) to select the propagation direction.

The estimated axon diameter index α along streamlines is different in the two fascicles, but

similar across SNR and tractography initialization techniques (see Table 2). However, α is always underestimated for the fascicle with the highest cylinder diameter, and overestimated for the fascicle with the lowest cylinder diameter. Although the cylinder diameter estimated at each segment is not the same as the ground truth, the estimation is consistent across segment and streamlines of the same fascicle. This can be observed in Figure 1 (d) where the fibre ODF peaks have a consistent α estimation with *AMICO* [Auría et al., 2015], both in single and multiple fibres populations. Table 2 shows that at high SNR, the standard deviation of the estimation of the axon diameter index α decreases. This decrease in the variability of the estimated α increases the overall quality of the tractography reconstruction, as shown by the *Tractometer* in Table 1. This stresses the importance of having high SNR data for microstructure estimation and consequently, microstructure informed tractography. Nevertheless, *AxTract* always increases valid connections and decreases invalid connections compared to conventional deterministic tractography, even at SNR=10.

Characterizing axon diameter index *in vivo*

AxTract enables the characterization of the axon diameter index α along white matter fascicles *in vivo*. The estimation of α with *AMICO* [Auría et al., 2015] along the tracking process with *AxTract* seems to be spatially coherent, as shown in Figures 2, 3 and 4, both on local estimation and on the median along streamlines. The value observed in the corpus callosum, see Figure 5 (a), follows the low-high-low trend observed in histology [Aboitiz et al., 1992], with lower values in the splenium and genu, and higher value in the body of the corpus callosum. However, as shown in Figures 5, this is visible only in the midsagittal slice of the corpus callosum. Alexander et al. [2010] suggested the trend observed in the midsagittal slice could be related to more complex axon geometry within those voxels, such as bending and fanning, not well supported by the *ActiveAx* model, and biasing the fitting. The *ActiveAx* model was later extended by Zhang et al. [2011b] to account for orientation dispersion using a Watson distribution. Their method better explains the data for the considered voxels, providing equally or more consistent agreement between the microstructure estimated and the observations from histology [Zhang et al., 2011b]. Nonetheless, similar estimates of the axon diameter index α were obtained for the midsagittal slice of the corpus callosum with the proposed model of the axonal dispersion. Recently, Ronen et al. [2013] reported axonal angular dispersion in the body of the corpus callosum that could bias the estimation of the axon diameter index α. This bias could also be a partial explanation for the discrepancy between the relative differences in the average α of different fascicles, shown in Figure 7, and the histological measures done by Liewald et al. [2014]. This could also be due to the limitation of histology which only allows for measuring axon diameters on a single slice [Liewald et al., 2014] while *AxTract* enables the overall quantification on the whole fascicle. Further investigation is needed to better understand why microstructure trends on whole fascicles differ from trends on a single slice, as well as the relationship between the axon diameter index α and axon physiology [Aboitiz et al., 1992; Alexander et al., 2010; Daducci et al., 2015; Debanne et al., 2011; Dyrby et al., 2012; Liewald et al., 2014; Ye et al., 2016; Zhang et al., 2011b]. Remarkably, *AxTract*, despite these limitations, is able to show consistent differences between fascicles in the mean axon diameter index α segment-wise across subjects (see Figure 7). Fascicles mean axon diameter index can also be computed *a posteriori* from the axon diameter index in the segment-wise orientation of streamlines obtained from conventional deterministic tractography. Additionally, fascicles mean axon diameter index can be obtained from streamline post-processing methods such as *MicroTrack* [Sherbondy et al., 2010] or *COMMIT* [Barakovic et al., 2016; Daducci et al., 2014]. These methods associate a white matter model to each streamline and optimize the model parameters of all streamlines

simultaneously to best fit the DW-MRI signal. They rely on the same hypothesis that microstructure features are consistent along the white matter fibres. In both cases, this provide an additional fascicle index that could be studied alongside other indices such as the apparent fibre density and the fractional anisotropy, to improve our understanding of brain connectivity and pathology.

Toward reducing invalid connections *in vivo*

The axon diameter index α changed the tracking direction mostly in voxels located in low angle crossing areas of the white matter, as shown on Figure 6. On average, these changes in direction happened in 19.0% of tracking steps with multiple directions available, which account for 2.5% of all tracking steps. This suggests that the direction picked by the conventional deterministic tractography is usually the direction that shows the less variation in α. Nonetheless, a single change in the propagation direction can affect the reconstruction of the whole fascicle. This is shown in Figure 7 (a), where *AxTract* increases the streamline count by an average of 6.3% across the selected fascicles for 34 subjects. This increase is obtained by solely changing the selection of the propagation direction with *AxTract*, keeping the same other tractography parameters. This increase in streamline count for a fascicle can be explained by three factors: 1) a decrease in erroneous streamlines not reaching the grey matter, 2) a decrease in erroneous streamlines connecting invalid grey matter regions or 3) streamlines connecting alternative valid grey matter regions from initial positions. Both factors 1) and 2) will improve the streamline reconstruction by overall increasing the valid connections. However, the observed increase of valid connections could be due to a decrease in valid connections from other existing fascicles of the brain (factor 3). We observed such a decrease in the streamline count for the arcuate fasciculus, see Figure 7 (a). Seeds forming arcuate fasciculus connections with conventional deterministic tractography might have formed other valid connections with *AxTract* (e.g. fascicles kissing or crossing with the arcuate fasciculus such as the superior longitudinal fasciculus). This reduction in the streamline count might also be attributed to more seeds forming invalid connections or erroneous streamlines due to errors in the axon diameter index estimation, making *AxTract* follow incorrect directions. Further investigation is needed to better understand the changes in the streamlines distribution *in vivo*. Nevertheless, this suggests that *AxTract* has a consistent effect on some of the reported fascicles across subjects. More realistic phantoms, such the one proposed for the ISMRM 2015 Tractography challenge (http://tractometer.org/ismrm_2015_challenge)[Maier-Hein et al., 2016] should also provide more insights in the potential of *AxTract*.

It is worth mentioning that we observed fascicles in some subjects with lower streamline coverage than we expected for both *AxTract* and the conventional deterministic tractography (e.g. the mid-posterior part of the corpus callosum and the right inferior fronto-occipital fasciculus of subject mgh_1001). In most cases, there were streamlines covering the expected fascicles area. However, these streamlines didn't fully agree the strict fascicles definition used to automatically obtained streamlines with *TractQuerier* (e.g. incomplete streamlines stopping in the white matter).

Limitations and future work

In the current implementation, the propagation direction is selected only by minimizing the change in the axon diameter index, given the directions within the maximum deviation angle θ. It is not clear which angle θ provides the optimal reconstruction throughout fascicles of the brain. It would be interesting to relax the angular criterion, especially with *AxTract* where two criteria (difference in axon diameter index and angular difference) are used in the selection of the propagation direction. In future work, *AxTract* could be extended to select the propagation direction using a distance function

combining both criteria (e.g. allowing high angular difference when the distance in axon diameter index is low).

AxTract approximates the axon diameter index of the fascicle being reconstructed using the median segment-wise α over a fixed distance of $5cm$. This parameter is of high importance as it affects the propagation direction selected by *AxTract*. If the distance parameter is too little, fascicles overlapping with the one being reconstructed will bias its axon diameter index estimation. This will cause the tractography to potentially follow erroneous propagation directions. Alternatively, if the distance parameter is to big, biological changes in the fascicle axon diameter distribution cannot be taking into account (e.g. branching or fanning). Again, this could lead to the tractography following erroneous directions. More research is needed to best select and adapt this parameter for the fascicle being reconstructed.

Finally, *AxTract* will directly benefit from improvements in local axon diameter acquisition, modelling and reconstruction techniques. In future work, it will be of interest to extend the current tracking algorithm to follow not only the median α of the fascicle, but to follow the α distribution of a fascicle [Assaf et al., 2008]. In particular, fascicles have a distribution of axon diameter that can partially overlaps, crosses and branches with other fascicles. Following the direction with the lowest change in α can results in an under-representation (or absence) of the smaller branching parts of the reconstructed fascicles. *AxTract* follows the directions having the most coherence in α, and as such, aims at reconstructing the main structure of the fascicles. Further improvements in the axon diameter distribution mapping could allows tractography to disentangle fascicles axon diameter distribution overlapping in a parallel direction and helps identify smaller branching structures. In addition, the estimation of α could be extended to more directions than the fibre ODF peaks. This requires new developments in axon diameter mapping methods, but would allow the use of α in probabilistic tractography algorithms [e.g. Behrens et al., 2007; Jeurissen et al., 2011] or global tractography frameworks [e.g. Fillard et al., 2009; Jbabdi et al., 2007; Kreher et al., 2008; Reisert et al., 2014, 2011].

Conclusion

To conclude, we presented *AxTract*, a novel algorithm to address the crossing/kissing problem of fascicles passing through areas of complex white matter configurations. *AxTract* uses axon diameter information to reduce ambiguities in the selection of the propagation direction, thus potentially reducing invalid connections and increasing valid connections produced by tractography algorithms. This was shown on simulations and on a group of 34 healthy subjects. *AxTract* is a framework and the first step towards advanced techniques able to incorporate tractography and microstructure imaging together. As microstructure modelling and reconstruction improve in the future, so will *AxTract*. This will enable the study of microstructure characteristics of white matter fascicles and go towards quantitative connectivity mapping.

Acknowledgements. This work has been supported in part by the European Union's Horizon 2020 Framework Programme for Research and Innovation under grant agreement 665667 (call 2015), by the European Research Council (ERC) under the Horizon 2020 research and innovation program (ERC Advanced Grant agreement No 694665: CoBCoM). and by the Natural Sciences and Engineering Research Council of Canada (NSERC). Human brain data for this project were provided by the Human Connectome Project (HCP; Principal Investigators: Bruce Rosen, M.D., Ph.D., Arthur W. Toga, Ph.D., Van J. Weeden, MD). HCP funding was provided by the National Institute of Dental and Craniofacial Research (NIDCR), the National Institute of Mental Health (NIMH), and the National

Institute of Neurological Disorders and Stroke (NINDS). HCP data are disseminated by the Laboratory of Neuro Imaging at the University of Southern California.

References

Aboitiz, F., Scheibel, a. B., Fisher, R. S., and Zaidel, E. (1992). Fiber composition of the human corpus callosum. *Brain research*, 598(1-2):143–153.

Alexander, D. C., Hubbard, P. L., Hall, M. G., Moore, E. A., Ptito, M., Parker, G. J., and Dyrby, T. B. (2010). Orientationally invariant indices of axon diameter and density from diffusion MRI. *NeuroImage*, 42:1374–1389.

Amitay, S. B., Lifshits, S., Barazany, D., and Assaf, Y. (2016). 3-Dimensional Axon Diameter Estimation of White Matter Fiber Tracts in The Human Brain. In *Organization for Human Brain Mapping*, Geneva, Switzerland.

Andersson, J., Xu, J., Yacoub, E., Auerbach, E., Moeller, S., and Ugurbil, K. (2012). A comprehensive Gaussian Process framework for correcting distortions and movements in diffusion images. In *International Symposium on Magnetic Resonance in Medicine*.

Assaf, Y. and Basser, P. J. (2005). Composite hindered and restricted model of diffusion (CHARMED) MR imaging of the human brain. *NeuroImage*, 27(1):48–58.

Assaf, Y., Blumenfeld-Katzir, T., Yovel, Y., and Basser, P. J. (2008). AxCaliber: a method for measuring axon diameter distribution from diffusion MRI. *Magnetic Resonance in Medicine*, 59:1347–1354.

Auría, A. R., Romascano, D. P. R., Canales-Rodriguez, E., Wiaux, Y., Dyrby, T. B., Alexander, D., Thiran, J.-P., and Daducci, A. (2015). Accelerated microstructure imaging via convex optimisation for regions with multiple fibres (amicox). In *IEEE International Conference on Image Processing*, Québec, Canada.

Avants, B. B., Tustison, N., and Song, G. (2009). Advanced normalization tools (ants). *Insight J*, 2:1–35.

Barakovic, M., Romascano, D., Dyrby, T., Alexander, D., Descoteaux, M., and Jean-Philippe Thiran, A. D. (2016). Assessment of bundle-specific axon diameter distributions using diffusion MRI tractography. In *Organization for Human Brain Mapping*, Geneva, Switzerland.

Barazany, D., Jones, D. K., and Assaf, Y. (2011). AxCaliber 3D. In *International Symposium on Magnetic Resonance in Medicine*, Montréal, Canada.

Basser, P. J., Pajevic, S., Pierpaoli, C., Duda, J., and Aldroubi, A. (2000). In vivo fiber tractography using DT-MRI data. *Magnetic Resonance in Medicine*, 44:625–632.

Behrens, T. E. J., Berg, H. J., Jbabdi, S., Rushworth, M. F. S., and Woolrich, M. W. (2007). Probabilistic diffusion tractography with multiple fibre orientations: What can we gain? *NeuroImage*, 34(1):144–155.

Burcaw, L. M., Fieremans, E., and Novikov, D. S. (2015). Mesoscopic structure of neuronal tracts from time-dependent diffusion. *NeuroImage*, 114:18–37.

Caruyer, E., Daducci, A., Descoteaux, M., Houde, J.-c., Thiran, J.-p., and Verma, R. (2014). Phantomas: a flexible software library to simulate diffusion MR phantoms. In *International Symposium on Magnetic Resonance in Medicine*, Milan, Italy.

Catani, M., Allin, M. P. G., Husain, M., Pugliese, L., Mesulam, M. M., Murray, R. M., and Jones, D. K. (2007). Symmetries in human brain language pathways correlate with verbal recall. *Proceedings of the National Academy of Sciences of the United States of America*, 104(43):17163–17168.

Côté, M.-A., Girard, G., Boré, A., Garyfallidis, E., Houde, J.-C., and Descoteaux, M. (2013). Tractometer: Towards Validation of Tractography Pipelines. *Medical Image Analysis*, 17(7):844–857.

Daducci, A., Canales-Rodríguez, E. J., Zhang, H., Dyrby, T. B., Alexander, D. C., and Thiran, J.-P. (2015). Accelerated Microstructure Imaging via Convex Optimization (AMICO) from diffusion MRI data. *NeuroImage*, 105:32–44.

Daducci, A., Dal Palu, A., Alia, L., and Thiran, J.-P. (2014). COMMIT: Convex Optimization Modeling for Micro-structure Informed Tractography. *IEEE Transactions on Medical Imaging*, pages 1–1.

Daducci, A., Dal Palú, A., Descoteaux, M., and Thiran, J.-P. (2016). Microstructure Informed Tractography: Pitfalls and Open Challenges. *Frontiers in Neuroscience*, 10:247.

Daducci, A., Dal Palu, A., Lemkaddem, A., and Thiran, J.-P. (2013). A convex optimization framework for global tractography. In *IEEE International Symposium on Biomedical Imaging*, pages 524–527.

Debanne, D., Campanac, E., Bialowas, A., Carlier, E., and Alcaraz, G. (2011). Axon physiology. *Physiological Reviews*, 91(2):555–602.

Dell'Acqua, F., Rizzo, G., Scifo, P., Clarke, R. A., Scotti, G., and Fazio, F. (2007). A model-based deconvolution approach to solve fiber crossing in diffusion-weighted MR imaging. *IEEE Transactions on Biomedical Engineering*, 54(3):462–472.

Dell'Acqua, F., Simmons, A., Williams, S., and Catani, M. (2010). Can Spherical Deconvolution give us more information beyond fibre orientation? Towards novel quantifications of white matter integrity. In *International Symposium on Magnetic Resonance in Medicine*, Stockholm, Sweden.

Dell'Acqua, F., Simmons, A., Williams, S. C., and Catani, M. (2013). Can spherical deconvolution provide more information than fiber orientations? Hindrance modulated orientational anisotropy, a true-tract specific index to characterize white matter diffusion. *Human Brain Mapping*, 34(10):2464–2483.

Descoteaux, M., Angelino, E., Fitzgibbons, S., and Deriche, R. (2007). Regularized, fast, and robust analytical Q-ball imaging. *Magnetic Resonance in Medicine*, 58(3):497–510.

Descoteaux, M., Deriche, R., Knösche, T. R., and Anwander, A. (2009). Deterministic and probabilistic tractography based on complex fibre orientation distributions. *IEEE Transactions on Medical Imaging*, 28(2):269–286.

Dyrby, T. B., Sø gaard, L. V., Hall, M. G., Ptito, M., and Alexander, D. C. (2012). Contrast and stability of the axon diameter index from microstructure imaging with diffusion MRI. *Magnetic Resonance in Medicine*, 721(2013):711–721.

Fan, Q., Witzel, T., Nummenmaa, A., Van Dijk, K. R., Van Horn, J. D., Drews, M. K., Somerville, L. H., Sheridan, M. A., Santillana, R. M., Snyder, J., Hedden, T., Shaw, E. E., Hollinshead, M. O., Renvall, V., Zanzonico, R., Keil, B., Cauley, S., Polimeni, J. R., Tisdall, D., Buckner, R. L., Wedeen, V. J., Wald, L. L., Toga, A. W., and Rosen, B. R. (2016). MGHUSC Human Connectome Project datasets with ultra-high b-value diffusion MRI. *NeuroImage*, 124:1108–1114.

Fick, R. H. J., Wassermann, D., Caruyer, E., and Deriche, R. (2016). MAPL: Tissue microstructure estimation using Laplacian-regularized MAP-MRI and its application to HCP data. *NeuroImage*, 134(1):365–385.

Fillard, P., Poupon, C., and Mangin, J.-F. (2009). A novel global tractography algorithm based on an adaptive spin glass model. In *International Conference on Medical Image Computing and Computer Assisted Intervention*, pages 927–934, London, United Kingdom.

Fonov, V., Evans, A. C., Botteron, K., Almli, C. R., McKinstry, R. C., and Collins, D. L. (2011). Unbiased average age-appropriate atlases for pediatric studies. *NeuroImage*, 54(1):313–327.

Garyfallidis, E., Brett, M., Amirbekian, B., Rokem, A., Van Der Walt, S., Descoteaux, M., and Nimmo-Smith, I. (2014). Dipy, a library for the analysis of diffusion MRI data. *Frontiers in Neuroinformatics*, 8.

Girard, G., Whittingstall, K., Deriche, R., and Descoteaux, M. (2014). Towards quantitative connectivity analysis: reducing tractography biases. *NeuroImage*, 98:266–278.

Greve, D. N. and Fischl, B. (2009). Accurate and robust brain image alignment using boundary-based registration. *NeuroImage*, 48(1):63–72.

Gudbjartsson, H. and Patz, S. (1995). The rician distribution of noisy mri data. *Magnetic Resonance in Medicine*, 34(6):910–914.

Hall, M. G. and Alexander, D. C. (2009). Convergence and parameter choice for Monte-Carlo simulations of diffusion MRI. *IEEE transactions on medical imaging*, 28(9):1354–1364.

Huang, S. Y., Nummenmaa, A., Witzel, T., Duval, T., Cohen-Adad, J., Wald, L. L., and McNab, J. A. (2015). The impact of gradient strength on in vivo diffusion MRI estimates of axon diameter. *NeuroImage*, 106:464–472.

Jbabdi, S., Sotiropoulos, S. N., Haber, S. N., Van Essen, D. C., and Behrens, T. E. (2015). Measuring macroscopic brain connections in vivo. *Nature Neuroscience*, 18(11):1546–1555.

Jbabdi, S., Woolrich, M. W., Andersson, J. L. R., and Behrens, T. E. J. (2007). A Bayesian framework for global tractography. *NeuroImage*, 37(1):116–129.

Jeurissen, B., Leemans, A., Jones, D. K. D. K., Tournier, J.-D. J. D., and Sijbers, J. (2011). Probabilistic fiber tracking using the residual bootstrap with constrained spherical deconvolution. *Human Brain Mapping*, 32(3):461–479.

Jolles, D., Wassermann, D., Chokhani, R., Richardson, J., Tenison, C., Bammer, R., Fuchs, L., Supekar, K., and Menon, V. (2016). Plasticity of left perisylvian white-matter tracts is associated with individual differences in math learning. *Brain Structure and Function*, 221(3):1337–1351.

Jones, D. K. (2010). Challenges and limitations of quantifying brain connectivity in vivo with diffusion MRI. *Imaging in Medicine*, 2(3):341–355.

Kaden, E., Kruggel, F., and Alexander, D. C. (2015). Quantitative mapping of the per-axon diffusion coefficients in brain white matter. *Magnetic Resonance in Medicine*, 75(9):1752–1763.

Keil, B., Blau, J. N., Biber, S., Hoecht, P., Tountcheva, V., Setsompop, K., Triantafyllou, C., and Wald, L. L. (2013). A 64-channel 3T array coil for accelerated brain MRI. *Magnetic Resonance in Medicine*, 70(1):248–258.

Kreher, B. W., Mader, I., and Kiselev, V. G. (2008). Gibbs tracking: a novel approach for the reconstruction of neuronal pathways. *Magnetic Resonance in Medicine*, 60(4):953–963.

Lebel, C. and Beaulieu, C. (2009). Lateralization of the arcuate fasciculus from childhood to adulthood and its relation to cognitive abilities in children. *Human Brain Mapping*, 30(11):3563–3573.

Liewald, D., Miller, R., Logothetis, N., Wagner, H.-J., and Schüz, A. (2014). Distribution of axon diameters in cortical white matter: an electron-microscopic study on three human brains and a macaque. *Biological Cybernetics*, 108(5):541–557.

Maier-Hein, K., Neher, P., Houde, J.-C., Cote, M.-A., Garyfallidis, E., Zhong, J., Chamberland, M., Yeh, F.-C., Lin, Y. C., Ji, Q., Reddick, W. E., Glass, J. O., Chen, D. Q., Feng, Y., Gao, C., Wu, Y., Ma, J., Renjie, H., Li, Q., Westin, C.-F., Deslauriers-Gauthier, S., Gonzalez, J. O. O., Paquette, M., St-Jean, S., Girard, G., Rheault, F., Sidhu, J., Tax, C. M. W., Guo, F., Mesri, H. Y., David, S., Froeling, M., Heemskerk, A. M., Leemans, A., Bore, A., Pinsard, B., Bedetti, C., Desrosiers, M., Brambati, S., Doyon, J., Sarica, A., Vasta, R., Cerasa, A., Quattrone, A., Yeatman, J., Khan, A. R., Hodges, W., Alexander, S., Romascano, D., Barakovic, M., Auria, A., Esteban, O., Lemkaddem, A., Thiran, J.-P., Cetingul, H. E., Odry, B. L., Mailhe, B., Nadar, M., Pizzagalli, F., Prasad, G., Villalon-Reina, J., Galvis, J., Thompson, P., Requejo, F., Laguna, P., Lacerda, L., Barrett, R., Dell'Acqua, F., Catani, M., Petit, L., Caruyer, E., Daducci, A., Dyrby, T., Holland-Letz, T., Hilgetag, C., Stieltjes, B., and Descoteaux, M. (2016). Tractography-based connectomes are dominated by false-positive connections. *bioRxiv*.

Malcolm, J. G., Shenton, M. E., and Rathi, Y. (2010). Filtered multitensor tractography. *IEEE Transactions on Medical Imaging*, 29(9):1664–75.

Matsui, J. T., Vaidya, J. G., Wassermann, D., Kim, R. E., Magnotta, V. A., Johnson, H. J., and Paulsen, J. S. (2015). Prefrontal cortex white matter tracts in prodromal Huntington disease. *Human Brain Mapping*, 36(10):3717–3732.

Novikov, D. S., Jensen, J. H., Helpern, J. A., and Fieremans, E. (2014). Revealing mesoscopic structural universality with diffusion. *Proceedings of the National Academy of Sciences*, 111(14):5088–5093.

Özarslan, E., Koay, C. G., Shepherd, T. M., Komlosh, M. E., İrfanoğlu, M. O., Pierpaoli, C., and Basser, P. J. (2013). Mean apparent propagator (MAP) MRI: A novel diffusion imaging method for mapping tissue microstructure. *NeuroImage*, 78:16–32.

Panagiotaki, E., Schneider, T., Siow, B., Hall, M. G., Lythgoe, M. F., and Alexander, D. C. (2012). Compartment models of the diffusion MR signal in brain white matter: A taxonomy and comparison. *NeuroImage*, 59(3):2241–2254.

Pestilli, F., Yeatman, J. D., Rokem, A., Kay, K. N., and Wandell, B. A. (2014). Evaluation and statistical inference for human connectomes. *Nature Methods*, 11:1058–1063.

Raffelt, D., Tournier, J.-D., Rose, S., Ridgway, G. R., Henderson, R., Crozier, S., Salvado, O., and Connelly, A. (2012). Apparent Fibre Density: A novel measure for the analysis of diffusion-weighted magnetic resonance images. *NeuroImage*, 59(4):3976–94.

Reisert, M., Kiselev, V. G., Dihtal, B., Kellner, E., and Novikov, D. S. (2014). MesoFT: Unifying Diffusion Modelling and Fiber Tracking. In *International Conference on Medical Image Computing and Computer-Assisted Intervention*, pages 201–208, Boston, United-States.

Reisert, M., Mader, I., Anastasopoulos, C., Weigel, M., Schnell, S., and Kiselev, V. (2011). Global fiber reconstruction becomes practical. *NeuroImage*, 54(2):955–962.

Ritchie, J. M. (1982). On the relation between fibre diameter and conduction velocity in myelinated nerve fibres. *Proceedings of the Royal Society of London. Series B, Containing papers of a Biological character. Royal Society (Great Britain)*, 217(1206):29–35.

Ronen, I., Budde, M., Ercan, E., Annese, J., Techawiboonwong, A., and Webb, A. (2013). Microstructural organization of axons in the human corpus callosum quantified by diffusion-weighted magnetic resonance spectroscopy of N-acetylaspartate and post-mortem histology. *Brain Structure and Function*, pages 1–13.

Salat, D. H., Greve, D. N., Pacheco, J. L., Quinn, B. T., Helmer, K. G., Buckner, R. L., and Fischl, B. (2009). Regional white matter volume differences in nondemented aging and Alzheimer's disease. *NeuroImage*, 44(4):1247–1258.

Savadjiev, P., Rathi, Y., Bouix, S., Smith, A. R., Schultz, R. T., Verma, R., and Westin, C.-F. (2014). Fusion of white and gray matter geometry: A framework for investigating brain development. *Medical Image Analysis*, 18(8):1349–1360.

Scherrer, B., Schwartzman, A., Taquet, M., Sahin, M., Prabhu, S. P., and Warfield, S. K. (2015). Characterizing brain tissue by assessment of the distribution of anisotropic microstructural environments in diffusion-compartment imaging (DIAMOND). *Magnetic Resonance in Medicine*, 76(3):963–977.

Sepehrband, F., Clark, K. A., Ullmann, J. F. P., Kurniawan, N. D., Leanage, G., Reutens, D. C., and Yang, Z. (2015). Brain tissue compartment density estimated using diffusion-weighted MRI yields tissue parameters consistent with histology. *Human Brain Mapping*, 36(9):3687–3702.

Setsompop, K., Kimmlingen, R., Eberlein, E., Witzel, T., Cohen-Adad, J., McNab, J. A., Keil, B., Tisdall, M. D., Hoecht, P., Dietz, P., Cauley, S. F., Tountcheva, V., Matschl, V., Lenz, V. H., Heberlein, K., Potthast, A., Thein, H., Van Horn, J., Toga, A., Schmitt, F., Lehne, D., Rosen, B. R., Wedeen, V., and Wald, L. L. (2013). Pushing the limits of in vivo diffusion MRI for the Human Connectome Project. *NeuroImage*, 80:220–233.

Sherbondy, A. J., Rowe, M. C., and Alexander, D. C. (2010). MicroTrack: an algorithm for concurrent projectome and microstructure estimation. In *International Conference on Medical Image Computing and Computer-Assisted Intervention*, pages 183–90, Beijing, China.

Smith, R. E., Tournier, J.-D., Calamante, F., and Connelly, A. (2013). SIFT: Spherical-deconvolution informed filtering of tractograms. *NeuroImage*, 67:298–312.

Song, S.-K., Yoshino, J., Le, T. Q., Lin, S.-J., Sun, S.-W., Cross, A. H., and Armstrong, R. C. (2005). Demyelination increases radial diffusivity in corpus callosum of mouse brain. *NeuroImage*, 26(1):132–140.

Thiebaut de Schotten, M., Ffytche, D. H., Bizzi, A., Dell'Acqua, F., Allin, M., Walshe, M., Murray, R., Williams, S. C., Murphy, D. G., and Catani, M. (2011). Atlasing location, asymmetry and inter-subject variability of white matter tracts in the human brain with MR diffusion tractography. *NeuroImage*, 54(1):49–59.

Thomas, C., Ye, F. Q., Irfanoglu, M. O., Modi, P., Saleem, K. S., Leopold, D. A., and Pierpaoli, C. (2014). Anatomical accuracy of brain connections derived from diffusion MRI tractography is inherently limited. *Proceedings of the National Academy of Sciences of the United States of America*, 111(46):16574–9.

Tournier, J.-D., Calamante, F., and Connelly, A. (2007). Robust determination of the fibre orientation distribution in diffusion MRI: non-negativity constrained super-resolved spherical deconvolution. *NeuroImage*, 35(4):1459–1472.

Tournier, J.-D., Calamante, F., and Connelly, A. (2012). MRtrix: Diffusion tractography in crossing fiber regions. *International Journal of Imaging Systems and Technology*, 22(1):53–66.

Tristán-Vega, A., Westin, C.-F., and Aja-Fernández, S. (2009). Estimation of fiber orientation probability density functions in high angular resolution diffusion imaging. *NeuroImage*, 47:638–650.

Tuch, D. (2004). Q-ball imaging. *Magnetic Resonance in Medicine*, 52:1358–1372.

Vernooij, M. W., Smits, M., Wielopolski, P. A., Houston, G. C., Krestin, G. P., and Van Der Lugt, A. (2006). Fiber density asymmetry of the arcuate fasciculus in relation to functional hemispheric language lateralization in both right- and left-handed healthy subjects: A combined fMRI and DTI study. *NeuroImage*, 35(3):1064–1076.

Wassermann, D., Makris, N., Rathi, Y., Shenton, M., Kikinis, R., Kubicki, M., and Westin, C.-F. (2016). The white matter query language: a novel approach for describing human white matter anatomy. *Brain structure & function*, pages 1–17.

Weinstein, D., Kindlmann, G., and Lundberg, E. (1999). Tensorlines: advection-diffusion based propagation through diffusion tensor fields. In *IEEE Visualization 1999*, volume 3, pages 249–253, San Fransisco, United-States.

Ye, L., Allen, W., Thompson, K., Tian, Q., Hsueh, B., Ramakrishnan, C., Wang, A.-C., Jennings, J. H., Adhikari, A., Halpern, C., Witten, I., Barth, A., Luo, L., McNab, J. A., and Deisseroth, K. (2016). Wiring and Molecular Features of Prefrontal Ensembles Representing Distinct Experiences. *Cell*, 165(7):1776–1788.

Zhang, H., Dyrby, T. B., and Alexander, D. C. (2011a). Axon Diameter Mapping in Crossing Fibers with Diffusion MRI. In *International Conference on Medical Image Computing and Computer-Assisted Intervention*, pages 82–89.

Zhang, H., Hubbard, P. L., Parker, G. J. M., and Alexander, D. C. (2011b). Axon diameter mapping in the presence of orientation dispersion with diffusion MRI. *NeuroImage*, 56(3):1301–15.

Zhang, H., Schneider, T., Wheeler-Kingshott, C. A., and Alexander, D. C. (2012). NODDI: Practical in vivo neurite orientation dispersion and density imaging of the human brain. *NeuroImage*, 61(4):1000–1016.

Zhang, Y., Brady, M., and Smith, S. (2001). Segmentation of brain MR images through a hidden Markov random field model and the expectation-maximization algorithm. *IEEE Transactions on Medical Imaging*, 20(1):45–57.

Axon Diameter Index Estimation

The framework *AMICO* (Accelerated Microstructure Imaging via Convex Optimization) [Auría et al., 2015; Daducci et al., 2015] provides the means to efficiently estimates microstructure information using a linear formulation. *AMICO* expresses the multi-compartment mapping problem as

$$\frac{\boldsymbol{S}}{S_0} = \Phi\mathbf{x} + \boldsymbol{\eta},$$

where $\boldsymbol{S} \in \mathbb{R}^N$ is the vector of diffusion weighted signal measurements, S_0 the signal without diffusion weighting, $\mathbf{x} \in \mathbb{R}^K$ the coefficients of the dictionary $\Phi \in \mathbb{R}^{N\times K}$ and $\boldsymbol{\eta} \in \mathbb{R}^N$ the acquisition noise [Daducci et al., 2015]. The dictionary Φ is built from different matrices:

$$\Phi = [\Phi^{iso} |\ \Phi_1^{intra} |\ \Phi_1^{extra} | \dots |\ \Phi_M^{intra} |\ \Phi_M^{extra}],$$

where $\Phi^{iso} \in \mathbb{R}^{N\times K_{iso}}$ are isotropic response functions accounting for free and isotropically restricted water [Panagiotaki et al., 2012] with diffusivity ranging from 3×10^{-3} to 1×10^{-3} mm^2/s, and $\Phi_i^{intra} \in \mathbb{R}^{N\times K_{intra}}$ the intra-axonal and $\Phi_i^{extra} \in \mathbb{R}^{N\times K_{extra}}$ extra-axonal compartments to account for the DW-MRI signal attenuation along the M fibre directions $\boldsymbol{d}_m$. The intra-axonal compartments Φ_i^{intra} models the DW-MRI signal decay of water molecules restricted within parallel cylinders [Alexander et al., 2010; Daducci et al., 2015; Dyrby et al., 2012; Panagiotaki et al., 2012] of diameter ranging from 2 to 10 μm. The intra-axonal diffusivity was fixed to 1.7×10^{-3} mm^2/s [Dyrby et al., 2012; Panagiotaki et al., 2012]. The parallel diffusivity of the extra-axonal compartments Φ_i^{extra} was also fixed to 1.7×10^{-3} mm^2/s, and distinct perpendicular diffusivity ranging from 0.06×10^{-3} to 0.42×10^{-3} mm^2/s [Daducci et al., 2015; Panagiotaki et al., 2012]. The model assumes no exchange between compartments.

Given the DW-MRI signal and a set of fibre directions, *AMICO* solves

$$\arg\min_{\mathbf{x}\geq 0} \frac{1}{2}\left\| \Phi\mathbf{x} - \frac{\boldsymbol{S}}{S_0} \right\|_2^2 + \lambda\frac{1}{2}\|\mathbf{x}\|_2^2, \quad \text{s.t.} \ \ \lambda > 0$$

where $\|\cdot\|_2^2$ is the ℓ_2 norm and the parameter λ controls the trade-off between the data and the regularization terms. Doing so, it enables the estimation of the mean diameter of cylinders along each fibre direction

$$\alpha_{\boldsymbol{d}_m} = \frac{\sum_j 2R_j \mathbf{x}_{i_j}^{intra}}{\sum_j \mathbf{x}_{i_j}^{intra}},$$

where $\mathbf{x}_{i_j}^{intra}$ is the volume fraction of the compartment $\Phi_{i_j}^{intra}$ corresponding to cylinder of radius R_j (μm) in the direction $\boldsymbol{d}_m$. *AMICO* uses up to three fibre directions in the estimation [Auría et al., 2015]. We refer to $\alpha_{\boldsymbol{d}_m}$ as the axon diameter index [Alexander et al., 2010; Auría et al., 2015; Dyrby et al., 2012].

Table 1: *Tractometer* evaluation on the simulated kissing dataset. Tractography initialization was done both in fascicles interfaces (100 streamlines per voxel; 18,800 streamlines) and in the white matter volume (20 streamlines per voxel; 22,400 streamlines).

	Tractography Algorithm											
	Initiated from the interface						Initiated from the white matter					
	AxTract			CDT			*AxTract*			CDT		
SNR	10	20	30	10	20	30	10	20	30	10	20	30
VC	72.1	87.2	90.5	55.9	52.5	53.9	60.9	71.3	73.9	54.1	54.7	55.3
IC	15.3	8.5	7.9	31.9	42.6	44.2	19.6	15.4	15.2	27.4	32.3	34.2
NC	12.7	4.3	1.7	12.2	4.9	1.9	19.6	13.3	10.9	18.6	13.0	10.5

Table 2: Axon diameter index α estimated on the simulated kissing dataset. The ground truth and the mean α estimated on both fascicles are reported in μm ($\pm$ standard deviation).

	SNR	Right fascicle	Left fascicle
Ground Truth		6.88	2.44
AxTract initiated from the interface	10	5.02 $\pm$ 0.39	3.86 $\pm$ 0.54
	20	5.09 $\pm$ 0.30	3.87 $\pm$ 0.52
	30	5.08 $\pm$ 0.29	3.87 $\pm$ 0.49
AxTract initiated from the white matter	10	4.92 $\pm$ 0.49	3.79 $\pm$ 0.55
	20	5.02 $\pm$ 0.39	3.80 $\pm$ 0.53
	30	4.99 $\pm$ 0.38	3.80 $\pm$ 0.52

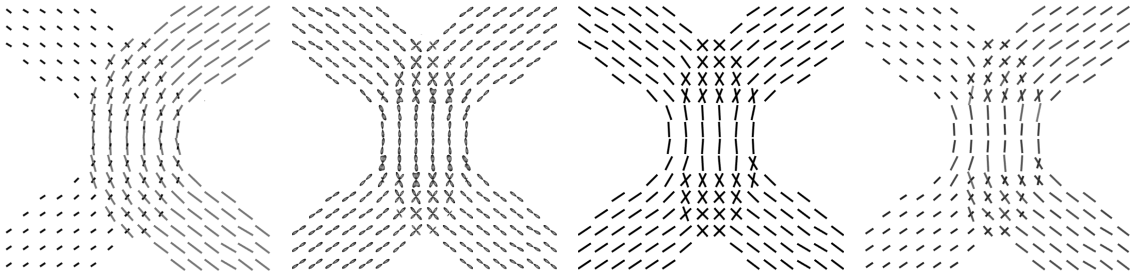

(a) Ground truth (b) fODFs (c) fODF peaks (d) peaks scaled with α

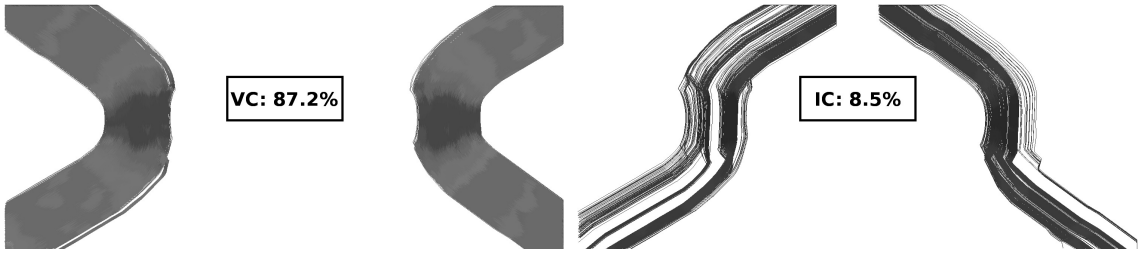

(e) *AxTract*

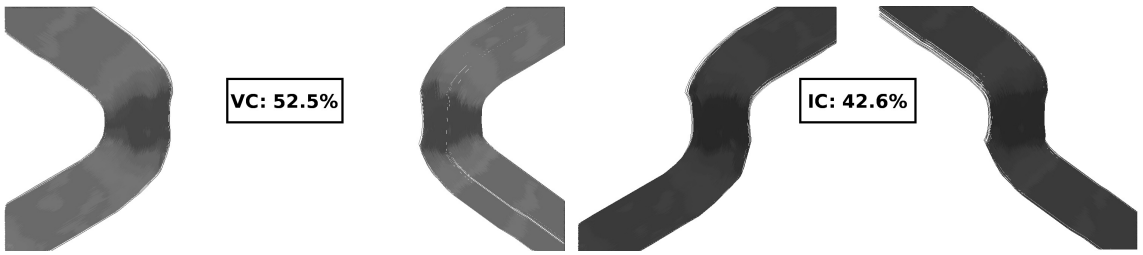

(f) CDT

Figure 1: Simulated kissing dataset ($SNR = 20$). The left fascicle and right fascicle have a mean axon diameter of $6.88\mu m$ and $2.44\mu m$, respectively. (a) shows the ground truth directions used to generate the data with their length scaled by the axon diameter index α, (b) the estimated fibre ODFs (fODFs), (c) the fibre ODF peaks and (d) the fibre ODF peaks with their length scaled by α, (e) show valid connections (VC) and invalid connections (IC) for *AxTract* and (f) show VC and IC for conventional deterministic tractography (CDT).

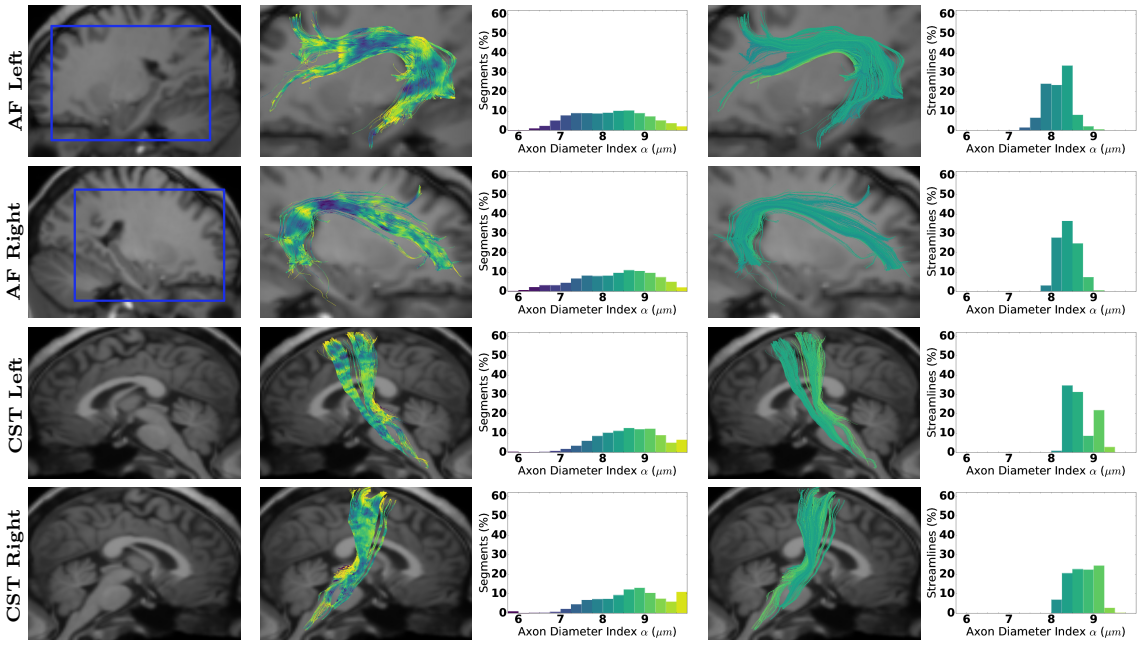

Figure 2: Axon diameter index α obtained with *AxTract* along the arcuate fasciculus (AF) and the corticospinal tract (CST). Column 1 shows a sagittal view of the T1-weighted image with the blue squares indicating the zooming areas for streamlines visualization. Column 2 shows fascicles coloured by α estimated per segment, with the histogram in column 3. Columns 4 and 5 show respectively fascicles with streamlines coloured by the whole-streamline median α and the histogram of whole-streamline median α, for all streamlines.

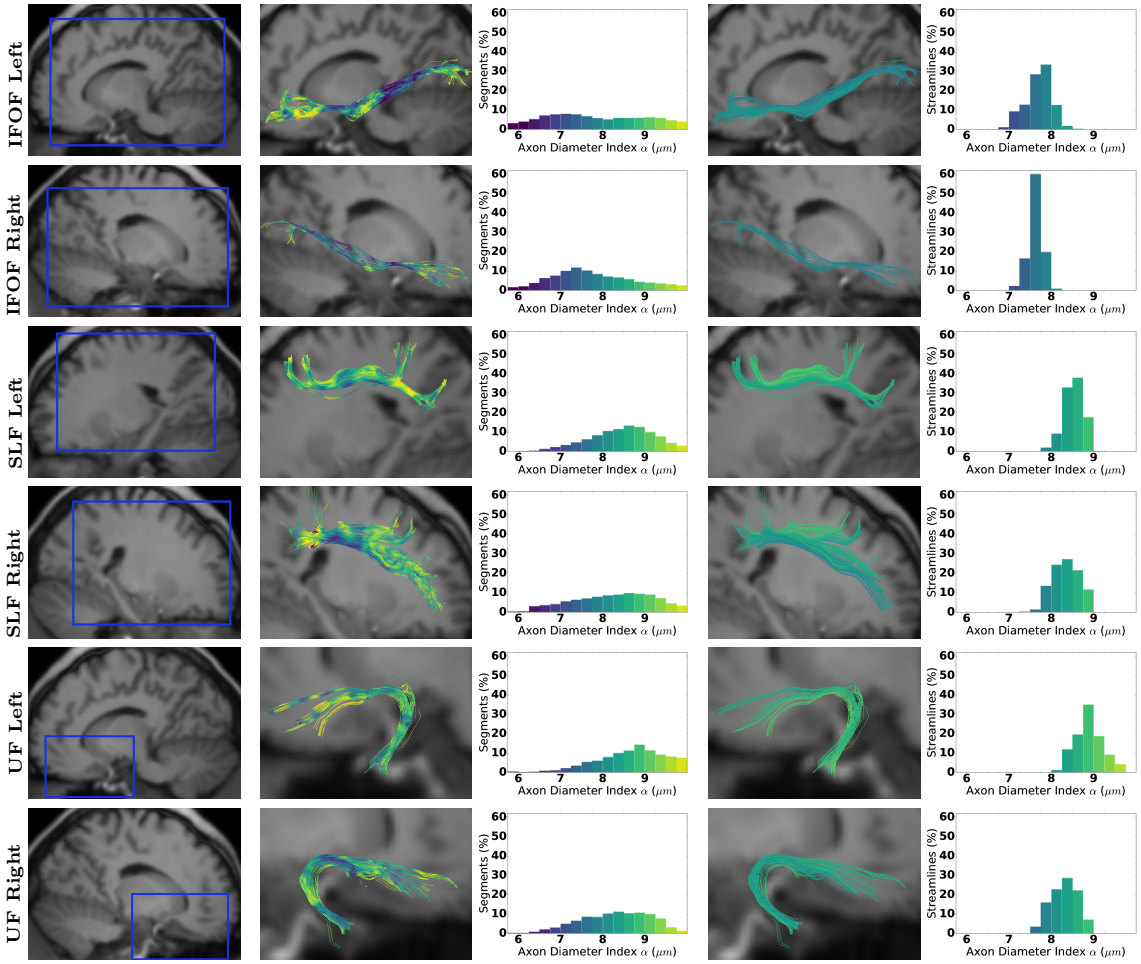

Figure 3: Axon diameter index α obtained with *AxTract* along the inferior fronto-occipital fasciculus (IFOF), the superior longitudinal fasciculus (SLF) and the uncinate fasciculus (UF). Column 1 shows a sagittal view of the T1-weighted image with the blue squares indicating the zooming areas for streamlines visualization. Column 2 shows fascicles coloured by α estimated per segment, with the histogram in column 3. Columns 4 and 5 show respectively fascicles with streamlines coloured by the whole-streamline median α and the histogram of whole-streamline median α, for all streamlines.

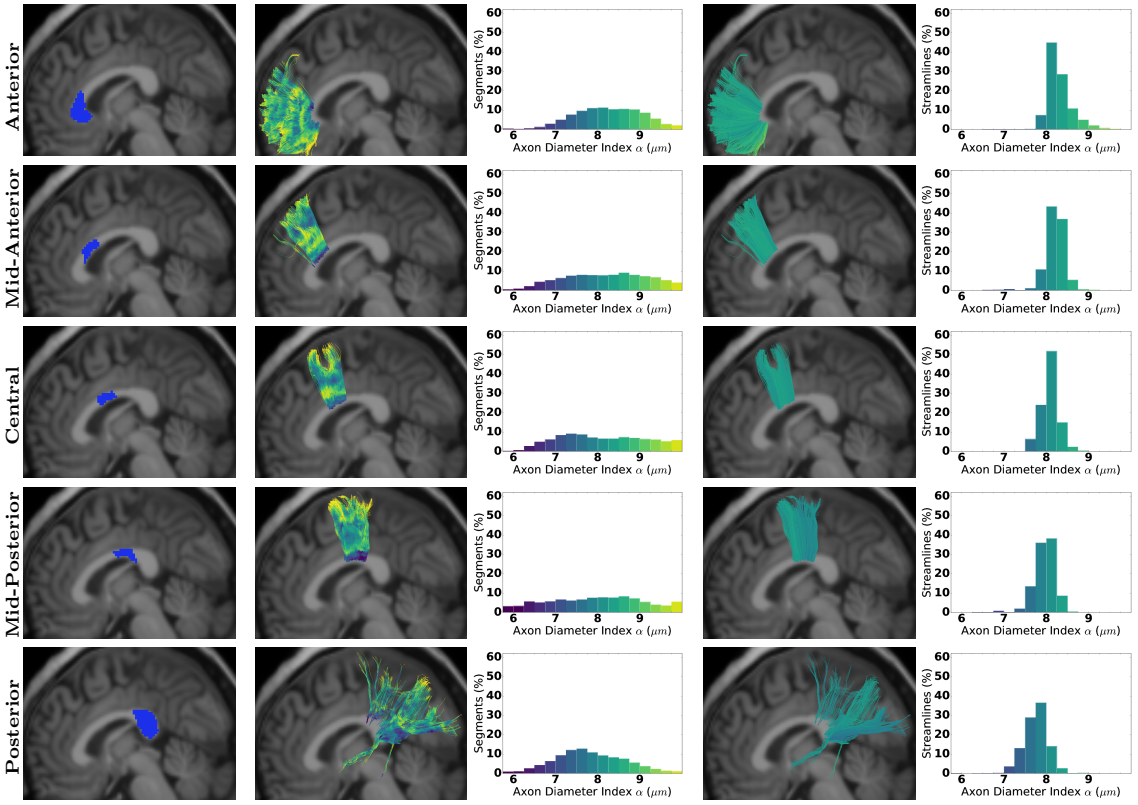

Figure 4: Axon diameter index α obtained with *AxTract* along the corpus callosum sub-fascicles. Column 1 shows the areas used to split the fascicle. Column 2 shows sub-fascicles coloured by α estimated per segment, with the histogram in column 3. Columns 4 and 5 show respectively fascicles with streamlines coloured by the whole-streamline median α and the histogram of whole-streamline median α, for all streamlines.

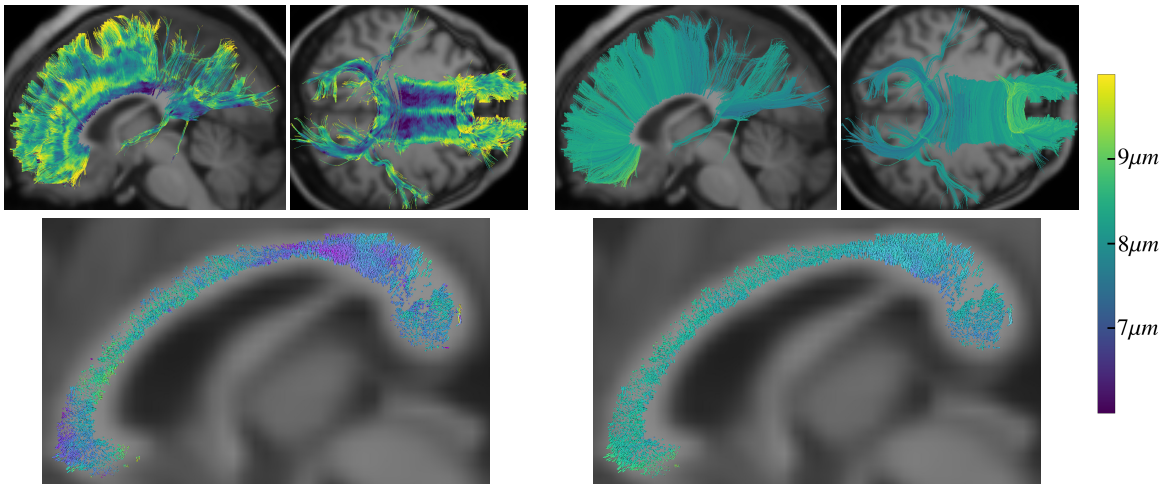

(a) Segment-wise colouring (b) Median colouring

Figure 5: Axon diameter index α obtained with *AxTract* of the corpus callosum. (a,b) Streamlines coloured using α estimated per segment and the whole-streamline median α, respectively. The top row show streamlines in lateral and inferior views and the bottom row show a sagittal cut of the streamlines going through the midsagittal slice of the corpus callosum.

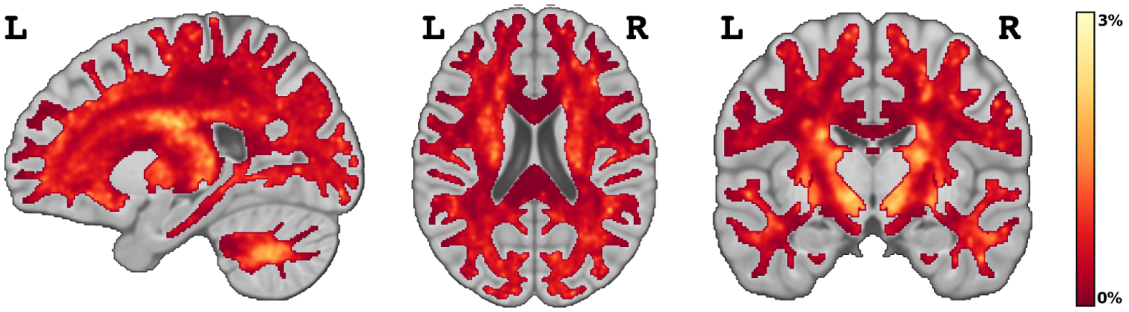

(a) Average occurrence map

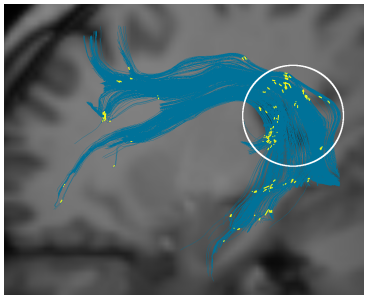

(b) Left Arcuate Fasciculus

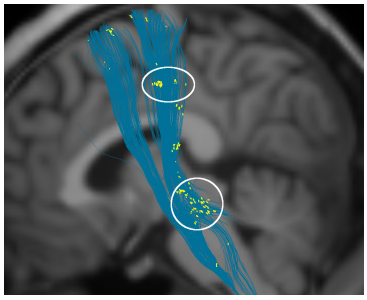

(c) Left Corticospinal Tract

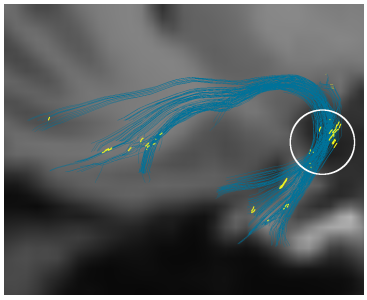

(d) Left Uncinate Fasciculus

Figure 6: Occurrence mapping of *AxTract* selecting a different propagation direction than conventional deterministic tractography (CDT). (a) Average occurrence map of *AxTract* selecting a different propagation direction than CDT over the 34 subjects. Individual subject occurrence maps were co-registered on the ICBM 152 average brain map, prior to the averaging. *AxTract* changed the propagation direction using the axon diameter index α in $19.0\% \pm 0.3$ of tracking steps with multiple directions available. (b,c,d) Occurrences of *AxTract* selecting a different propagating direction than CDT on three fascicles of one subject (yellow segments). The white ellipses highlight crossing areas where the use of the axon diameter index α modified the tractography.

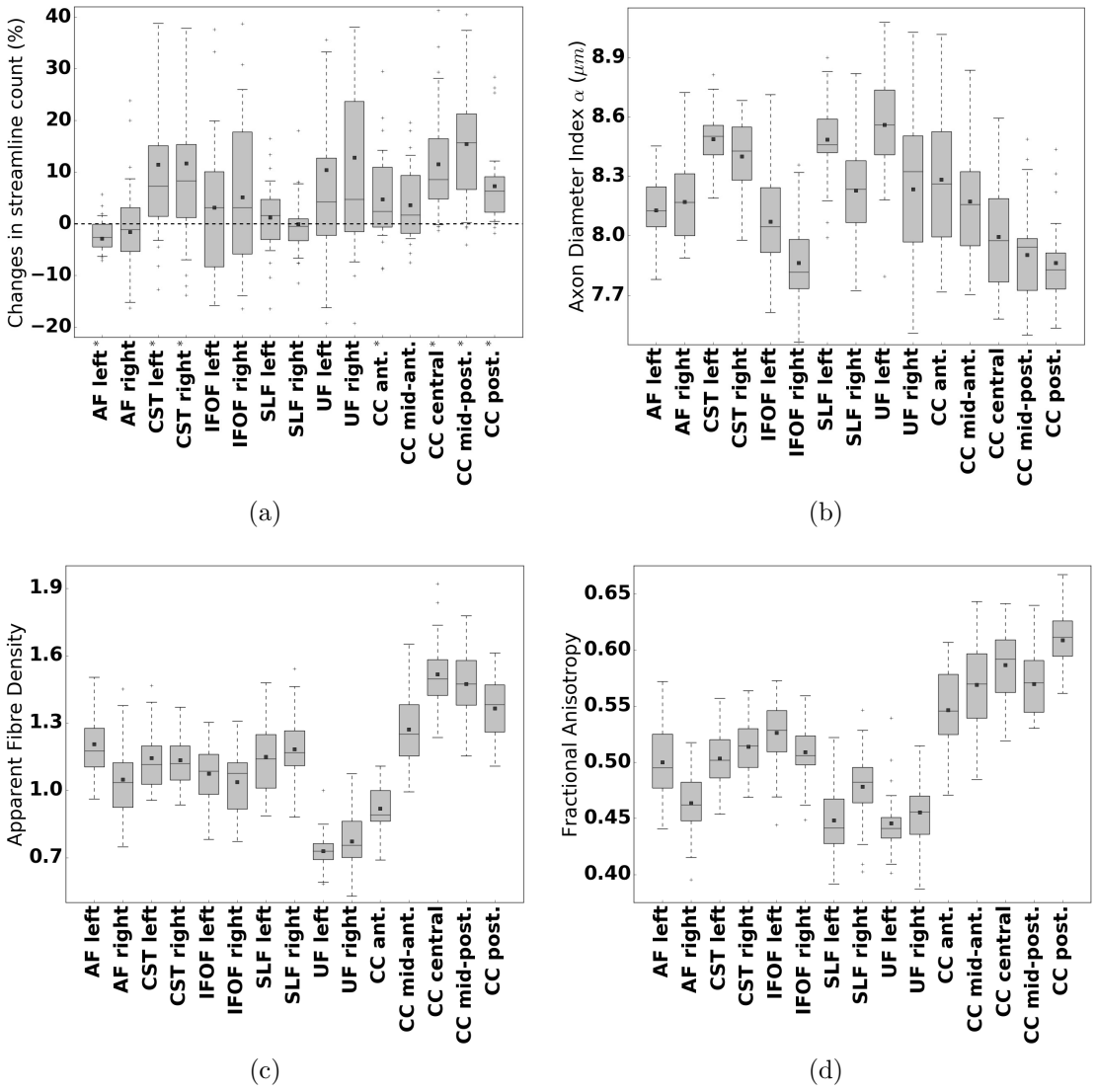

Figure 7: Fascicle property distributions of 34 healthy subjects. (a) Percentage change in the number of streamlines between *AxTract* and conventional deterministic tractography ($\frac{AxTract-CDT}{CDT} \times 100$). Fascicle with significant increase or decrease in streamline count are marked with an asterisk (*). (b) The mean axon diameter index α, (c) the mean apparent fibre density and (d) the mean fractional anisotropy, along streamline fascicles of 34 healthy subjects, obtained with *AxTract*. Results are shown for six fascicles: the arcuate fasciculus (AF), the corticospinal tract (CST), the inferior fronto-occipital fasciculus (IFOF), the superior longitudinal fasciculus (SLF), the uncinate fasciculus (UF) and the corpus callosum (CC). The CC is split in 5 sub-fascicles using the *FreeSurfer* parcellation (anterior, mid-anterior, central, mid-posterior, posterior) and *TractQuerier*. Projection and association fascicles are reported for each hemisphere. The black line indicates the median, the square indicates the mean, the box extends from the first and third quartile and the whiskers are at the 5th and 95th percentile of the distribution.